



**HAL**  
open science

## Predicting carbon diffusion in cementite from first principles

Océane Buggenhoudt, Thomas Schuler, Chu Chun Fu, Jean-Luc Bechade

► **To cite this version:**

Océane Buggenhoudt, Thomas Schuler, Chu Chun Fu, Jean-Luc Bechade. Predicting carbon diffusion in cementite from first principles. *Physical Review Materials*, 2021, 5, pp.063401. 10.1103/PhysRevMaterials.5.063401 . cea-03350631

**HAL Id: cea-03350631**

**<https://cea.hal.science/cea-03350631>**

Submitted on 21 Sep 2021

**HAL** is a multi-disciplinary open access archive for the deposit and dissemination of scientific research documents, whether they are published or not. The documents may come from teaching and research institutions in France or abroad, or from public or private research centers.

L'archive ouverte pluridisciplinaire **HAL**, est destinée au dépôt et à la diffusion de documents scientifiques de niveau recherche, publiés ou non, émanant des établissements d'enseignement et de recherche français ou étrangers, des laboratoires publics ou privés.

## Predicting carbon diffusion in cementite from first principles

Océane Buggenhoudt,\* Thomas Schuler, Chu-Chun Fu , and Jean-Luc Béchade 

Université Paris-Saclay, CEA, Service de Recherches de Métallurgie Physique, F-91191 Gif-sur-Yvette, France



(Received 18 January 2021; accepted 19 May 2021; published 1 June 2021)

Combining first-principles calculations with recently developed statistical physics tools, we determine carbon diffusion mechanisms and the resulting diffusion coefficients in pure-Fe and weakly alloyed  $M_3C$  cementites. The predicted coefficients in  $Fe_3C$  are in good agreement with experimental measurements of carburization rate in ferritic steels. In our proposed diffusion mechanisms, C migrates by jumps between interstitial sites rather than via the C Frenkel pair mechanism, as proposed by previous studies based on semiempirical simulations. In the alloyed cementites, the C diffusion can be slowed down due to the presence of Mn solutes up to 500 K, while it is mostly unaffected by the addition of Mo or Cr solutes.

DOI: [10.1103/PhysRevMaterials.5.063401](https://doi.org/10.1103/PhysRevMaterials.5.063401)

### I. INTRODUCTION

The presence of precipitates, such as carbides, in metallic alloys has a strong impact on the mechanical properties of these materials. They can act as obstacles to impede the motion of dislocations. As a result, the presence of carbides such as  $M_{23}C_6$  or MC can strengthen the matrix of ferritic-martensitic steels and prevent the sliding of grain boundaries [1]. In addition, the precipitation of carbides influences strongly the thermal conductivity of heat-treatable steels [2]. The stability of carbides is reduced by irradiation. Experimental studies report the precipitation of new carbide phases around pre-existing carbides under ion irradiation or high temperature neutron irradiation [1,3], as well as the dissolution [1,4] and the amorphisation of pre-existing carbide phases under ion irradiation [1]. Yet, it is difficult to provide a quantitative explanation of these observations in out-of-equilibrium conditions since the equilibrium thermodynamic and diffusion properties of carbides are still poorly known. Cementite ( $Fe_3C$ ) is a common carbide, often found in model iron alloys and industrial ferritic steels, in particular in materials for the nuclear industry such as 16MND5 pressurized water reactor vessels steels. In order to better understand the kinetics of cementite nucleation and growth process, or the transition mechanism from this carbide to another one, it is essential to understand its atomic diffusion properties. Since interstitial diffusion generally requires a lower activation energy than the vacancy-mediated diffusion of the metallic atoms, as a first step, we address the carbon diffusion in cementite.

There are relatively few experimental studies on C diffusion in  $Fe_3C$ . All of them are carburization experiments, in which C diffusion coefficients in  $Fe_3C$  were indirectly obtained through the dependence of cementite growth rate on the carbon activity in the gas phase. Hillert and Sharp [5] first studied carbon diffusion in cementite at 1138K by imposing a low C activity ( $a_c = 1.3$ ) at the cementite surface. They evaluated the carbon diffusion coefficient in  $Fe_3C$  at

$D_C \approx 1.27 \times 10^{-14} \text{ m}^2 \text{ s}^{-1}$ . Ozturk's group [6,7] investigated the kinetics of cementite formation by carburizing fine iron powders at 723 K. They estimated the C diffusion coefficient in  $Fe_3C$  as a function of carbon activity (from  $a_c = 4.3$  to  $a_c = 20$ ), and obtained diffusion coefficients ranging from  $10^{-20}$  to  $10^{-19} \text{ m}^2 \text{ s}^{-1}$ . More recently, Schneider and Inden [8] carburized pure iron samples at 773 K. They increased the carbon activity up to  $a_c = 4580$ . At carbon activities  $a_c > 150$ , Hägg carbides ( $Fe_5C_2$ ) formed on top of cementite. They obtained  $D_C \approx 6.05 \times 10^{-18} \text{ m}^2 \text{ s}^{-1}$  in  $Fe_3C$  cementite. Additional experimental results are cited in Ref. [9], as a private communication. They were obtained from carburization experiments on pure iron, for temperature ranging from 843 to 983 K. The corresponding C diffusion coefficients vary from  $3.5 \times 10^{-17}$  to  $1.3 \times 10^{-15} \text{ m}^2 \text{ s}^{-1}$ . Ozturk *et al.* suggested that the C atom migrates via interstitial or interstitialcy mechanism because its diffusion coefficient in  $Fe_3C$  increases with the C activity in the gas. Yet, such experimental studies cannot provide detailed information about the migration mechanism at the atomic scale. Moreover, the C diffusion coefficients are measured indirectly and only at rather high temperatures (above 723 K). In addition, the results rely on a cementite growth model which involves several assumptions. Therefore, accurate atomistic modeling provides useful and complementary insights into the diffusion coefficients of C in  $Fe_3C$ , and the underlying diffusion mechanisms.

Levchenko *et al.* performed a molecular dynamic (MD) simulation of carbon diffusion in cementite [9], employing empirical potentials. In their study, they distinguish C atoms forming the cementite structure (which we will refer to as intrinsic C atoms from now on) located on triangular prismatic sites, from interstitial C atoms in octahedral sites. Levchenko *et al.* found that, as thermally activated events, originally intrinsic C atoms move to nearby interstitial sites, this way creating C Frenkel pairs. Furthermore, the nearest distance between an intrinsic C site and an interstitial octahedral site in cementite (2.55 Å) is lower than the distance between two intrinsic C (3.02 Å), or two interstitial octahedral sites (3.36–3.37 Å). Therefore, they suggested that carbon diffusion in cementite results from sequences of C intrinsic - C interstitial

\*oceane.buggenhoudt@cea.fr

- C intrinsic jumps. They calculated C diffusion coefficients in cementite between 1273 and 1373 K and obtained values ranging between  $1.66 \times 10^{-12}$  and  $4.19 \times 10^{-12} \text{ m}^2 \text{ s}^{-1}$ . Assuming that the temperature dependence of these coefficients follows an Arrhenius law, these values are in reasonable agreement with an extrapolation of the experimental data to high temperatures. The formation energy found for the C Frenkel pairs was 0.3 eV/atom, while the migration energy was approximately 1.3 eV/atom for temperatures between 1273 and 1373 K. These MD simulations were performed at very high temperatures (between 1273 and 1373 K), and employed empirical potentials. The obtained concentration of C Frenkel pairs was high: the authors predicted an equilibrium fraction of C atoms in interstitial sites (and thus the same fraction of intrinsic C vacancies) between 0.21 and 0.23. It is worth checking, via first-principles calculations, the efficiency of their proposed mechanism, and the possible occurrence of other mechanisms, in particular at lower temperatures (for instance, in the temperature range of the carburization experiments).

On the other hand, previous first-principles study by C. Jiang *et al.* [10] investigated in detail the thermodynamic properties of point defects in pure-Fe cementite. They also calculated energy barriers of the jump of an isolated C vacancy and a C interstitial, which are the dominant defects and the proposed diffusing species in C-depleted and C-rich regimes, respectively. However, diffusion coefficients involving long-range diffusion of C atoms were not computed in that study.

In Fe alloys, metallic solutes commonly substitute certain Fe atoms in cementite precipitates. Experimental studies on the fabrication of bulk cementite through mechanical alloying and spark plasma sintering have shown that Cr, Mn, Mo, and V form alloyed cementite and stabilize it [11]. It is therefore relevant to determine the influence of alloying elements on C diffusion in cementite.

In this study, we present a detailed investigation of C migration mechanisms, and determine the C diffusion coefficients in  $\text{Fe}_3\text{C}$  and weakly alloyed cementite  $(\text{Fe}_{1-x}\text{M}_x)_3\text{C}$ , with  $M = \text{Mo}, \text{Cr}, \text{and Mn}$ , which are common alloying elements in ferritic steels, employed in nuclear reactors, for example. This paper is organized as follows: in Sec. II, we present the density functional theory (DFT) calculation setup, the method to determine the diffusion coefficients, as well as structural characteristics of cementite. Then, DFT results on the energetics of the various C interstitial sites found are detailed in Sec. III A, along with the migration barriers of all the relevant C migration paths, that are used as input data for the KineCluE code to compute C diffusion coefficients in cementite (Sec. III B). Finally, the influence of a substitutional Mo, Mn or Cr atom in the metallic sublattice on the energetics, the migration barriers and the diffusion coefficients of C is discussed in Sec. III C.

## II. METHODS

### A. DFT calculation details

First-principles calculations were performed using density functional theory (DFT) with the projected augmented wave (PAW) method [12,13] as implemented in the VASP (Vienna

*ab initio* simulation package) code [13–15]. 3*d* and 4*s* electrons are considered as valence electrons for Fe, Cr, and Mn atoms, and 4*d* and 5*s* electrons for Mo, while 2*s* and 2*p* states are considered for C. We employed the generalized gradient approximation (GGA) with the Perdew-Burke-Eruzerhof (PBE) scheme [16]. All the calculations were spin polarized within the collinear approximation. The plane-wave basis cutoff was set to 500 eV. The convergence cutoff for the electronic self-consistency loop was set to  $\Delta E = 10^{-6}$  eV. Except when otherwise mentioned, all the results presented below are obtained using a  $2 \times 2 \times 2$  orthorhombic supercell of cementite containing 128 or  $128 + 1$  atoms, and a  $5 \times 4 \times 5$  *k*-point grid, following the Monkhorst-Pack scheme [17]. The Methfessel-Paxton broadening scheme [18] with a 0.1 eV width was used. Atomic position, cell shape and size were fully relaxed to ensure a maximum residual force of 0.02 eV/Å and a maximum residual stress of 3 kbar.

To investigate the C interstitial migration, the energy barrier between a given initial and a final configuration was calculated using the nudged elastic band (NEB) methods [19,20]. We use at least three images between two given energy minima. These NEB calculations were performed at constant volume, adopting the lattice vectors of the fully relaxed cementite supercell.

For all the C jumps, the attempt frequency ( $\nu_0$ ) was approximated by that of octahedral C migration in bcc-Fe, the saddle-point configuration being the C at a tetrahedral site. It was calculated in the framework of the Vineyard transition state theory [21] within the harmonic approximation. We used a 128-atom bcc cell to determine the phonon frequencies with a  $4 \times 4 \times 4$  *k*-point grid. Both the octahedral and tetrahedral C configurations were initially relaxed to have a maximum residual force of less than 0.005 eV/Å.

We also performed phonon calculations in order to determine the free formation energy of C Frenkel pairs in cementite. Vibrational entropies were obtained within the harmonic approximation from the frozen phonon calculations in  $2 \times 1 \times 2$  cementite supercells using VASP and PHONOPY [22]. Before the phonon calculations, the cementite supercells were first fully relaxed with a maximum residual force of 0.001 eV/Å and a maximum residual stress of 1 kbar.

### B. Determination of diffusion coefficients

We want to study the kinetic properties of a C atom in cementite. The C diffusion coefficient in cementite is given by

$$D = D_0 \exp\left(\frac{-Q}{k_B T}\right), \quad (1)$$

with  $Q$  the activation energy,  $T$  the temperature and  $k_B$  the Boltzmann constant. Since diffusion in cementite is not random,  $D_0$  can be expressed as

$$D_0 = \frac{na^2}{6} \nu_0 f, \quad (2)$$

with  $a$  the jump length,  $n$  a geometrical factor for the number of equivalent jump paths and  $f$  the correlation factor. The energy barriers appearing in the expression of  $D$ , as well as the attempt frequency  $\nu_0$  are calculated with DFT.

We want to estimate the diffusivity of carbon in cementite. DFT calculations provide valuable information about migration and formation energies. Yet, in most cases, this data alone is not sufficient to evaluate mass-transport properties because the average mobility of a species is the result of all possible kinetic trajectories with their respective statistical weight. The integration of all possible trajectories is performed using the open-source code KineCluE [23,24] which automates the self-consistent mean field theory [25] to compute transport coefficients from the knowledge of the crystal structure, the available jump mechanisms for the C interstitial and information about the energetic landscape of the system. Within the KineCluE framework, the competition between various jump mechanisms as well as the interaction between C and other alloying elements are included [26–28].

As explained in the introduction, we also want to study the influence of an alloying element on C diffusivity in cementite. Under the approximation that the system is dilute in interstitial C and substitutional solute  $M$  ( $M = \text{Cr}, \text{Mo}, \text{Mn}$ ), we use the kinetic cluster expansion [24,27] formalism to compute the effect of cementite alloying on carbon diffusivity to first order in alloying elements concentration:

$$\bar{D}_C([\bar{M}]) = \frac{[C]D_C + [MC]D_p}{[\bar{C}]}, \quad (3)$$

where  $\bar{D}_C$  is the average C diffusion coefficient,  $[\bar{M}]$  and  $[\bar{C}]$  are the nominal solute and interstitial carbon concentrations, respectively,  $[C]$  is the concentration of isolated (i.e., far from alloying elements) interstitial carbon,  $[MC]$  is the concentration of solute-interstitial carbon pair,  $D_C$  is the diffusion coefficient of a single interstitial C atom in  $\text{Fe}_3\text{C}$  cementite, and  $D_p$  is the diffusion coefficient of an interstitial carbon atom around a solute  $M$ . All concentrations are given per cementite unit formula  $\text{Fe}_3\text{C}$ . These concentrations are obtained by using an approximation of the low-temperature expressions for dilute system [26,29], and solving the following coupled equations for given nominal concentrations:

$$\begin{aligned} [\bar{C}] &= [C] + [MC] = Z_C Y_C + Z_{MC} Y_C Y_M, \\ [\bar{M}] &= [M] + [MC] = Z_M Y_M + Z_{MC} Y_C Y_M, \end{aligned} \quad (4)$$

where the  $Y_\alpha = \exp(\mu_\alpha/k_B T)$  variables are the unknown of this system of equations, and the chemical potentials are taken as the energy required to create an interstitial carbon atom at an octahedral site or a  $M_{\text{II}}$  substitutional solute (the structure of cementite is detailed in Sec. II C). With these references in mind, the monomer partition functions read

$$\begin{aligned} Z_C &= 1 + \exp(-\Delta E_C/k_B T), \\ Z_M &= 2 + \exp(-\Delta E_M/k_B T), \end{aligned} \quad (5)$$

where  $\Delta E_C$  is the energy difference between a carbon atom forming a dumbbell at a cementite carbon site and a carbon atom being at an interstitial octahedral site.  $\Delta E_M$  is the energy difference between configurations where  $M$  is inserted at a  $M_{\text{II}}$  or  $M_{\text{I}}$  substitutional site. For  $Z_{MC}$  in Eq. (4), we chose a pair partition function to encompass all configurations that were computed *ab initio*, which means all configurations where the distance between the solute and the carbon atom are below 5.83 Å. This choice makes sense as long as carbon-solute

binding energies can be assumed to be zero beyond this distance.

If we pick the same definition of the pair cluster in KineCluE (setting the kinetic range to the same cutoff distance), we would not have converged diffusion coefficients because kinetic correlations always extend beyond thermodynamic interactions. But if we extend the kinetic range to a larger value, However, we would have inconsistent definitions between the thermodynamic and kinetic definition of the cluster, and we would also include monomer contributions into the diffusion coefficient of C around the solute. To solve this issue, we consider that a calculation to a larger kinetic radius (therefore a larger partition function) can be written as the sum of a pair contribution (defined by the 5.83 Å cutoff distance) and a monomer contribution. We can do the same calculation while setting all interactions between carbon and solute to zero, which will allow us to remove the monomer contribution with the same geometry. Under these considerations, we define the carbon diffusivity around a solute as

$$D_p(r_k) = D_C + \frac{Z(r_k)}{Z_{MC}} (D_C(r_k) - \bar{D}_C(r_k)), \quad (6)$$

where  $Z(r_k)$  is the partition function obtained by setting the kinetic range to  $r_k$ ,  $D_C(r_k)$  is the C diffusion coefficient around a solute computed with kinetic range  $r_k$ , and  $\bar{D}_C(r_k)$  is similar except that all carbon-solute interactions are set to zero. The C diffusion coefficient around a solute  $D_p(r_k)$  defined this way converges quickly with  $r_k$  and any  $r_k$  value larger than 9 Å will give the same value.

### C. Cementite structure

Cementite ( $\text{Fe}_3\text{C}$ ) crystallises in the orthorhombic space group  $Pnma$  (No. 62) with 4 formulas unit per unit cell [30]. Theoretical and experimental lattice parameters are given in Table I. The unit cell contains four 4c Fe atoms ( $\text{Fe}_{\text{I}}$ ) and eight 8d Fe atoms ( $\text{Fe}_{\text{II}}$ ). The four intrinsic 4c C atoms are located in triangular prismatic interstices of the Fe sub-lattice, with six nearest Fe atoms. Both  $\text{Fe}_{\text{I}}$  and  $\text{Fe}_{\text{II}}$  are 14-coordinated with twelve Fe and two C nearest neighbors (nn) for  $\text{Fe}_{\text{I}}$ , and eleven Fe and three C nn for  $\text{Fe}_{\text{II}}$ . The three lattice vectors ( $a$ ,  $b$  and  $c$ ) of the orthorhombic unit cell of cementite are respectively parallel to the  $[11\bar{1}]$ ,  $[112]$ , and  $[110]$  directions in a bcc-Fe cell (Table I).  $\text{Fe}_3\text{C}$  is ferromagnetic in its ground state with an experimental Curie temperature of 460 K [31] or 483–484K [32],[33]. Older experimental studies also reported some values between 473 and 513 K [34,35]. Please note that carburization experiments described above were all performed above the Curie temperature, while, as an approximation, all our calculations are carried out at the magnetic ground state of cementite. An accurate atomistic prediction of the impact of magnetic transition on carbon diffusion requires a significant amount of additional work [36], therefore, it is beyond the scope of this study. This approximation will be discussed in Sec. III B.

## III. RESULTS

### A. Properties of C interstitials in $\text{Fe}_3\text{C}$

First of all, we searched for empty volumes in the cementite structure, in order to identify potential C interstitial sites

TABLE I. Non exhaustive list of previous theoretical and experimental assessments of Fe<sub>3</sub>C lattice parameters.

Method [Ref]	Lattice parameters ( <i>a</i> , <i>b</i> , <i>c</i> ) (Å)	Fe magnetic moment ( $\mu_B$ ) Fe <sub>I</sub> , Fe <sub>II</sub>	Formation energy (eV/f.u. <sup>*</sup> )
DFT:			
VASP, PAW, GGA, 0 K [this work]	5.036, 6.721, 4.479	1.96, 1.88	0.204 (Fe bcc, graphite)
VASP, PAW, GGA, 0 K [37]	5.0289, 6.7262, 4.4823	2.006, 1.909	0.194 (Fe bcc, graphite)
CASTP, USSP, LDA, 0 K [38]	4.8190, 4.4774, 4.2805	1.990, 1.915	
CASTP, USSP, GGA, 0 K [38]	5.0080, 6.7254, 4.4650	1.990, 1.915	
WIEN2K, FP-LAPW, GGA, 0 K [39]	5.0679, 6.7137, 4.5133	1.97, 1.96	
VASP, PAW, GGA, 0 K [40]	5.04, 6.72, 4.48	1.96, 1.89	
VASP, PAW, GGA, 0 K [41]	5.036, 6.724, 4.480	1.87	
VASP, PAW, GGA, 0 K [42]	5.035, 6.716, 4.480	1.92, 1.84	0.243 (Fe bcc, graphite)
VASP, PAW, GGA, phonon calc. 298 K [42]	5.053, 6.745, 4.4503	1.92, 1.84	
VASP, PAW, GGA, 0 K [43]	5.024, 6.754, 4.478	1.82	0.18 (Fe bcc, graphite)
LMTO, LDA, 0 K [44]	5.089, 6.743, 4.523	7.92 <sup>a</sup> , 13.92 <sup>a</sup>	
Experimental:			
X-ray diffraction, 298 K [45]	5.090, 6.748, 4.523		
X-ray diffraction, 298 K [46]	5.091, 6.7434, 4.526		
X-ray diffraction, 298 K [47]	5.0896, 6.7443, 4.5248		
Neutron diffraction, 4.2 K [48]	5.082, 6.733, 4.512		
Neutron diffraction, 298 K [48]	5.081, 6.753, 4.515		

<sup>a</sup>Total on-site moment, d contribution only.

<sup>\*</sup>f.u.: formula unit.

in Fe<sub>3</sub>C. To do this, we created a grid of sampling points in the cementite unit cell, and determined the lowest distance between each point and an Fe or C atom in the cementite. The sampling points presenting large lowest distances are likely low-energy C interstitial sites. As a result, we identified five types of interstitial sites: octahedral sites, three nonequivalent tetrahedral sites (labeled T1, T2, and T3) and square-based pyramidal sites. T1 interstitial sites (4c) do not follow the same symmetry as T2 and T3 sites (8d). T2 and T3 sites do not have the same number of Fe<sub>I</sub> or Fe<sub>II</sub> nearest neighbors. These interstitial sites are represented in Fig. 1. In a previous study, Jiang *et al.* [40] also investigated interstitial sites in cementite. In their study, they predicted the existence of oc-

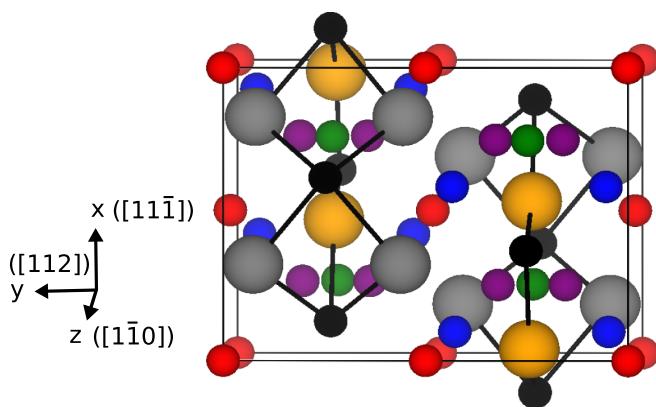


FIG. 1. Crystal structure of Fe<sub>3</sub>C cementite. Larger atoms are Fe atoms. Fe<sub>I</sub> atoms are in orange, while Fe<sub>II</sub> atoms are in grey. Smaller atoms are C atoms. C atoms forming the ideal cementite structure (C intrinsic atoms) are in black. Interstitial octahedral sites for C are in red. T1, T2, and T3 sites are in green, blue, and purple, respectively.

tahedral, T1, T2, and T3 sites. To be fully comprehensive, we also considered the formation of C dumbbells. For the study of diffusion in cementite, relevant dumbbells are centered on intrinsic C-atom positions and oriented along the [010] or [101] directions. Table II summarizes energetic and geometric information about the investigated C sites in cementite.

In order to investigate the relative stability of a C atom in each of these interstitial sites, we relaxed each C interstitial configuration in a  $2 \times 2 \times 2$  cementite Fe<sub>96</sub>C<sub>33</sub> supercell. The formation energy of Fe<sub>3</sub>C without interstitial is defined by

$$E^f(n(\text{Fe}_3\text{C})) = E(n(\text{Fe}_3\text{C})) - 3n\mu_{\text{Fe}}(\text{bcc}) - n\mu_{\text{C}}(\text{graph}), \quad (7)$$

where  $E(n(\text{Fe}_3\text{C}))$  is the total energy of the cementite cell. In our case, the DFT calculations were made in a 128 atoms cell, hence  $n = 8$ .  $\mu_{\text{Fe}}(\text{bcc})$  is the chemical potential of iron in ferromagnetic bcc iron and  $\mu_{\text{C}}(\text{graph})$  is the chemical potential of carbon in graphite. At 0 K,  $\mu_{\text{C}}(\text{graph})$  is the total energy per C atom in graphite and  $\mu_{\text{Fe}}(\text{bcc})$  is the total energy per Fe atom in bcc iron. In this study, we used  $\mu_{\text{C}}(\text{graph}) = E_{\text{C}}(\text{graph}) = -9.226$  eV and  $\mu_{\text{Fe}}(\text{bcc}) = E_{\text{Fe}}(\text{bcc}) = -8.238$  eV, obtained through DFT calculations. The graphite reference energy does not include Van der Waals corrections. For Fe<sub>3</sub>C cementite, we obtained a formation energy value of 0.204 eV/f.u., in good agreement with previous studies (see Table I).

The formation energy of a C interstitial in Fe<sub>3</sub>C cementite,  $E^f(\text{C}_{\text{int}}$  in  $n(\text{Fe}_3\text{C})$ ), is given by

$$E^f(\text{C}_{\text{int}} \text{ in } n(\text{Fe}_3\text{C})) = E(n(\text{Fe}_3\text{C}) + \text{C}_{\text{int}}) - E(n(\text{Fe}_3\text{C})) - \mu_{\text{C}}, \quad (8)$$

$E(n(\text{Fe}_3\text{C}) + \text{C}_{\text{int}})$  is the total energy of the cementite cell with an additional C interstitial and  $\mu_{\text{C}}$  is the chemical potential of carbon in a given reference state. We calculated the formation energy of a C interstitial in cementite with respect

TABLE II. Formation energy with respect to cementite and geometrical characteristics of a C interstitial at various interstitial sites in Fe<sub>3</sub>C cementite.

C site	$E^f(\text{C}_{\text{int}} \text{ in } \text{Fe}_3\text{C})$ (eV)	Lowest C <sub>int</sub> -Fe or C <sub>int</sub> -C distance before (after) relaxation (Å)	C <sub>int</sub> -C distance before (after) relaxation (Å)	C <sub>int</sub> Voronoi volume in the Fe <sub>3</sub> C relaxed cell (Å <sup>3</sup> )
Octa	0.64	1.79 (1.87)	2.55 (2.73)	6.05
T1	3.20	1.51 (1.79)	1.96 (1.99)	5.55
T2	2.62	1.51 (1.77)	1.96 (2.40)	5.40
T3	2.39	1.43 (1.77)	1.97 (2.32)	5.53
A dumbbell (along the <i>xz</i> plane)	2.34	1.51 (1.44)	1.51 (1.44)	5.88/5.59
B dumbbell (along <i>y</i> )	1.98	1.30 (1.42)	1.30 (1.42)	5.42

to intrinsic C atoms in cementite. Therefore,  $\mu_c = \mu_c(\text{Fe}_3\text{C})$ . At  $T = 0$  K and zero pressure, we have

$$E(n(\text{Fe}_3\text{C})) = 3n\mu_{\text{Fe}}(\text{Fe}_3\text{C}) + n\mu_c(\text{Fe}_3\text{C}), \quad (9)$$

Assuming that the cementite precipitate is in equilibrium with the bcc iron matrix, ( $\mu_{\text{Fe}}(\text{Fe}_3\text{C}) = \mu_{\text{Fe}}(\text{bcc})$ ), we combine the equations above to get

$$\begin{aligned} E^f(\text{C}_{\text{int}} \text{ in } \text{Fe}_3\text{C})_{\text{wrt Fe}_3\text{C}} &= E(n(\text{Fe}_3\text{C}) + \text{C}_{\text{int}}) \\ &\quad - E(n(\text{Fe}_3\text{C})) - E^f(\text{Fe}_3\text{C}) \\ &\quad - \mu_c(\text{graph}). \end{aligned} \quad (10)$$

The formation energies of the C interstitial sites calculated with respect to Fe<sub>3</sub>C are shown Table II. Because of their very high formation energy (6.16 eV), the square-based pyramidal sites were not considered further in this study. The octahedral sites were found to be the energetically most favorable, with a formation energy of 0.64 eV with respect to cementite. This result is in good agreement with Ref. [40], in which Jiang *et al.* used DFT to compare interstitial sites formation energies. Like us, they found that octahedral sites are energetically more favorable, followed by T3, T2, and T1 interstitial sites. In Levchenko *et al.* study [9], all the C interstitial sites considered are indeed the octahedral sites. If we compare the properties of each interstitial sites (Tables II and III), C octahedral interstitial sites are associated with the larger lowest-distance to another atom of the structure, the highest Voronoi volume and the higher average magnetic moments of the nearest Fe neighbors. It is well known that the insertion of a C interstitial in bcc Fe decreases the magnetic moment magnitude on the nearby Fe atoms [49,50]. Similarly, there is

also a magnetic moment reduction on the nearest-neighbor Fe atoms of a C interstitial in cementite. The resulting values are given in Table III.

We also considered the possible formation of C Frenkel pairs in cementite. To this end, we investigated all the possible pairs of a C intrinsic vacancy and a C in an octahedral site, for distances lower than the distance between two neighboring octahedral interstitial sites (3.36 Å). The formation energy of a C Frenkel pair defect in cementite  $E^f(\text{C}_{\text{int}} + \text{C}_v \text{ in } n(\text{Fe}_3\text{C}))$  is given by

$$\begin{aligned} E^f(\text{C}_{\text{int}} + \text{C}_v \text{ in } n(\text{Fe}_3\text{C})) &= E(\text{C}_{\text{int}} + \text{C}_v \text{ in } n(\text{Fe}_3\text{C})) \\ &\quad - E(n(\text{Fe}_3\text{C})) \end{aligned} \quad (11)$$

with  $E(\text{C}_{\text{int}} + \text{C}_v \text{ in } \text{Fe}_3\text{C})$  the total energy of the simulation cell containing the C Frenkel pair and  $E(n(\text{Fe}_3\text{C}))$  the total energy of the same Fe<sub>3</sub>C cell without any defect. The lowest distances between an intrinsic site and octahedral interstitial site are 2.55, 2.65, and 3.09 Å, with a formation energy of 1.01, 1.10, and 1.22 eV, respectively. While the 0.30 eV formation energy estimated in Levchenko *et al.* molecular dynamics study [9] is more than three times lower than our DFT values.

### B. C diffusion in Fe<sub>3</sub>C

The octahedral interstitial sites form a slightly tetragonal network with 3.37 Å between nearest-neighbor octahedral sites along the [101] and  $[\bar{1}01]$  directions, and 3.36 Å between nearest-neighbor octahedral sites along the *y* direction. Diffusion of a C interstitial in Fe<sub>3</sub>C is assumed to occur from one octahedral site to another, while the

 TABLE III. C-nearest Fe distances and average nearest Fe magnetic moments for a C atom at interstitial sites in Fe<sub>3</sub>C. In Fe<sub>3</sub>C without interstitial, Fe<sub>I</sub> atoms and Fe<sub>II</sub> magnetic moments are 1.96μ<sub>B</sub> and 1.88μ<sub>B</sub>, respectively.

Interstitial site	Number of nearest Fe neighbors Fe <sub>I</sub> /Fe <sub>II</sub>	C-Fe distances after relaxation (Å)	Average magnetic moment of Fe nearest neighbors (μ <sub>B</sub> )
Octa	2/4	between 1.87 and 1.91	1.63
T1	2/2	1.79-1.87 resp	1.13
T2	1/3	between 1.77 and 1.92	1.40
T3	2/2	between 1.77 and 1.92	1.33
A dumbbell (along the <i>xz</i> plane)	2/3 and 1/4	between 1.89 and 2.05 and 1.87 and 1.99	1.80/1.83
B dumbbell (along <i>y</i> )	2/3 and 2/3*	between 1.84 and 2.03	1.79

\*The 2 Fe<sub>I</sub> nearest neighbors are the same for both C forming a dumbbell.

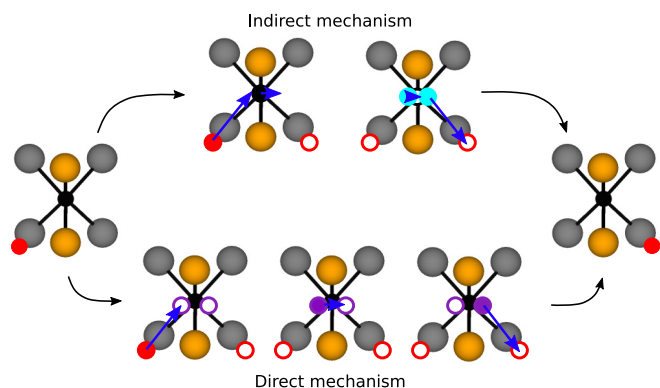


FIG. 2. Schematic view of indirect and direct C interstitial migration mechanisms in  $\text{Fe}_3\text{C}$ . Filled circles denote occupied sites, empty circles are vacant sites. Intrinsic C sites are in black,  $\text{Fe}_I$  sites are in orange and  $\text{Fe}_{II}$  sites are in grey. C octahedral interstitial sites are in red, T3 interstitial sites are in purple and dumbbells are in cyan.

other interstitial sites are possible metastable or saddle-point positions. We investigated two migration mechanisms: (i) a direct-interstitial mechanism, and (ii) an indirect mechanism via successive exchanges between interstitial and intrinsic C atoms. In the direct migration mechanism, a C interstitial atom simply jumps from one octahedral site to another. In the case of an indirect mechanism, an interstitial C atom jumps to replace an intrinsic cementite C atom, and the “kicked-out” atom jumps to a nearby interstitial octahedral position. A schematic view of these two migration mechanisms is given in Fig. 2. The resulting migration barriers, given in Table IV, lie between 2.13 and 2.54 eV. The lowest migration barrier was found for a direct mechanism along the  $xz$  plane in cementite (see Fig. 3). The lowest-energy barrier for the indirect jump mechanism (2.16 eV) is associated with a jump along the  $y$  axis and involves the energetically most favorable dumbbell configuration (B dumbbell along  $y$ ). Along the indirect migration path considered, the dumbbell configurations are intermediate local minima. Jiang *et al.* [10] attempted to determine the minimum energy path and migration barrier for C diffusion in cementite. They considered both vacancy and interstitial mechanisms. For the latter, they considered the jump of a C atom between two neighboring octahedral sites, in the  $y$  direction and along the  $xz$  plane. Using first-principles calculations in small 32-atom supercells, their calculated energy barriers are 2.29 and 2.27 eV, respectively. The authors did not detail the

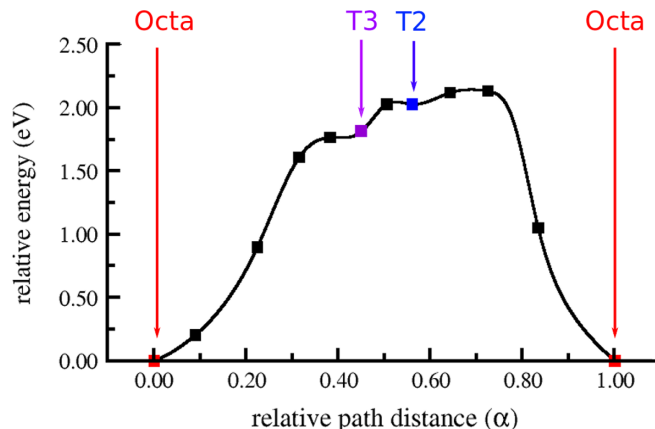


FIG. 3. Minimum energy path for the Octa - T3 - T2 - Octa direct jump mechanism along the  $xz$  plane in  $\text{Fe}_3\text{C}$ . The C interstitial (in red) goes from an octahedral site to another octahedral site, passing through two tetrahedral sites.

corresponding migration paths, but these values are closed to our 2.16 eV and 2.13 eV barriers calculated in the same directions.

For a comparison with the MD study by Levchenko *et al.* [9], please note that they did not consider the same migration mechanisms as in this work. As mentioned in the introduction, they found that C diffusion in cementite comes from the formation of C Frenkel pair defects in cementite, inducing a chain of C intrinsic-C interstitial-C intrinsic jumps. This mechanism relies on a high concentration of C Frenkel pairs. However, according to our DFT prediction (see Sec. III A), their interatomic potentials greatly underestimate the formation energy of C Frenkel pairs, which leads to a large overestimation of the number of Frenkel defects in cementite. Since the 0.3 eV formation energy was obtained from MD simulations at very high temperatures (between 1273 and 1373 K), we investigated the effect of the vibrational entropy on the formation of C Frenkel pairs. To that end, we performed phonons calculations via DFT. Since such calculations are very CPU expensive in these low-symmetry systems, we focused on the case of the energetically most favorable Frenkel pair (with the lowest C intrinsic - C octahedral interstitial distance). As a result, the free energy of formation only decreases from 1.01 eV at 0 K to 0.89 eV at 1273 K, and 0.88 eV at 1373 K, compared to 0.3 eV from the MD study. The formation energy of several neighboring Frenkel

TABLE IV. Summary of relevant jump mechanisms of a C interstitial and their associated energy barriers in  $\text{Fe}_3\text{C}$  cementite.

Jump mechanism	Path	Energy barrier (eV)
Indirect	Octa - B Dumbbell - Octa along $y$ axis	2.16
	Octa - A Dumbbell - Octa along the $xz$ plane	2.38
Direct	Octa - T3 - T2 - Octa along the $xz$ plane	2.13
	Octa - T3 - T3 - Octa along $y$ axis	2.46
	Octa - T3 - T1 - T3 - Octa along $y$ axis*	2.54
	Octa - T1 - Octa along $y$ axis*	2.54

\*The Octa - T3 - T1 - T3 - Octa and Octa - T1 - Octa migration path along  $y$  are ultimately the same. Moreover, they are just a less likely variation of the Octa - T3 - T3 - Octa migration path and thus were not considered as inputs for the KineCluE code.

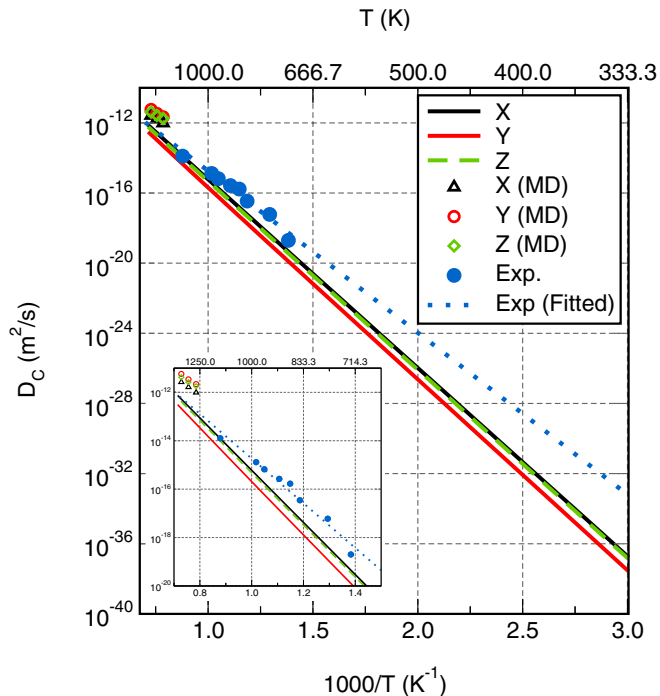


FIG. 4. Arrhenius plot of diffusion coefficients of a C interstitial in  $\text{Fe}_3\text{C}$  cementite. The diffusion coefficients in all 3 cementite directions are plotted and compared with experimental data [5–9] (in blue). Empty symbols correspond to the values obtained by semiempirical MD [9].

pairs could be lower than the formation energy of a single Frenkel pair. However, the number of close Frenkel pairs configurations to explore is too large to provide a comprehensive DFT study. Nonetheless, we considered several configurations of 2 Frenkel pairs, and calculated formation energies (per pair) around 0.86 eV. This value is the average on three configurations where the  $C_{\text{int}} - C_{\text{int}}$  distances (before relaxation) are 5.03, 3.36, and 3.36 Å; and the  $C_V - C_V$  distances (before relaxation) are 3.63, 5.10, and 3.03 Å. The lowest calculated formation energy, 0.75 eV, corresponds to the configuration with the lowest  $C_{\text{int}} - C_{\text{int}}$  and  $C_V - C_V$  distances among the configurations tested. Such diffusion mechanism is therefore unlikely, even at high temperature. In fact, in the carburization experiments, the carbon activity in the vapor phase was tuned to provide interstitial carbon atoms in  $\text{Fe}_3\text{C}$ . That is why, at variance with Levchenko *et al.*, we do not consider any C interstitial formation energy, but just the C migration energies between octahedral interstitial sites, for the C diffusion activation energy.

The DFT migration mechanisms and their associated energy barriers were used as inputs for the KineCluE code in order to compute the C diffusion coefficient in each direction, as shown in Fig. 4. We assumed the same attempt frequency for all the C jumps to be the one of an isolated C octahedral jump in bcc Fe for which we obtained an activation energy of 0.86 eV and an attempt frequency of 30.64 THz (corresponding to a diffusion prefactor of  $D_0 = 4.09 \times 10^{-7} \text{ m}^2 \text{ s}^{-1}$ ) in a 128 atom bcc cell. Previous *ab initio* studies by Jiang *et al.* [51] and Domain *et al.* [52] calculated attempt frequencies of 10.79 THz and 15.69 THz ( $D_0 = 1.44 \times 10^{-7} \text{ m}^2 \text{ s}^{-1}$  and

$D_0 = 2.13 \times 10^{-7} \text{ m}^2 \text{ s}^{-1}$ ) using the Einstein approximation. Simonovic *et al.* [53] used both the dynamical matrix calculation and the Einstein approximation to obtain 12.44 THz and 16.18 THz ( $D_0 = 1.66 \times 10^{-7} \text{ m}^2 \text{ s}^{-1}$  and  $D_0 = 2.16 \times 10^{-7} \text{ m}^2 \text{ s}^{-1}$ ), respectively. However, Simonovic *et al.* used a small cell (32 + 1 atoms). Overall, our  $D_0$  value is in good agreement with experimental studies ( $D_0$  included between  $1.67 \times 10^{-7}$  and  $2.0 \times 10^{-6} \text{ m}^2 \text{ s}^{-1}$ ) [54–60].

The obtained diffusion coefficients are in good agreement with the few carburization experimental data detailed in the introduction (blue dots Fig. 4). C diffusion in cementite is found to be slightly anisotropic, with the lowest diffusion coefficient along the y axis. In this direction,  $D_C$  is between approximately 2.5 and 4 times slower than in the x and z directions, for temperatures included between 500 and 1000 K. C diffusion is faster in the x direction, with  $D_C$  very close in the z direction. This slight anisotropic behavior is due to a small difference between the lowest energy barrier along the xz plane (2.13 eV) and the lowest energy barrier in the y direction (2.16 eV). Even if the nearest distance between two C octahedral interstitials is slightly smaller in the y direction (3.36 Å instead of 3.37 Å), a C interstitial jumping in this direction must go through the C intrinsic atoms. As a result, the C interstitial migration in the y direction can either take place through an indirect mechanism, or a longer Octa - T3 - T3 - Octa direct mechanism. In both cases, the required energy is larger than for a direct migration path along the xz plane.

Reference [9] also reported an anisotropic carbon diffusion, but with the lowest diffusion coefficient in the x direction. Overall, Levchenko *et al.* with C diffusion via Frenkel pairs overestimates the diffusion coefficients of carbon in cementite (by a factor of 10 approximately), while with our interstitial diffusion mechanisms, the calculated diffusion coefficients are slightly lower than the experimental results (also by a factor of 10 approximately). A detailed comparison between the activation energies and the pre-exponential factors is given in Table V. Overall, the experimental activation energy and pre-exponential factors are included between our values and MD values. Note that the correlation factors that we obtain range between 0.75 and 1.00 (see Fig. 5), which demonstrates the fact that C atoms are not performing a random-walk on the network of interstitial sites and that the importance of correlation effects depends on the diffusion direction. Overall, there is no correlation effect in the y and z directions ( $f \cong 1$ ), whereas the correlation factor is generally smaller along x.

As explained in Sec.II C, an atomistic study of cementite properties across the magnetic transition is beyond the scope of our study. Nevertheless, we estimated the impact of the paramagnetism in cementite on the formation energies of a C interstitial in an octahedral or a T3 site. To this end, we performed additional calculations using the previously relaxed ferromagnetic cementite structures (with and without a C interstitial), but with a special quasirandom structure (SQS) of Fe magnetic moments. Then, we replaced the total energies of the second and third terms of Eq. (10) by the total energies of the same cell, but with the Fe atoms in the paramagnetic state. Since the carburization experiments (with the exception of Hillert and Sharp work [5]) were performed

TABLE V. Activation energy (Q) and pre-exponential factors ( $D_0$ ) of carbon diffusion in cementite according to Arrhenius approximations of our study, Levchenko *et al.*'s MD study [9] and various experimental data [5–9].

Direction	Our study			MD study [9]			Exp. studies ([5–9])
	x	y	z	x	y	z	average
Q (eV)	2.13	2.17	2.13	1.50	1.45	1.26	1.83
$D_0$ ( $\text{m}^2 \text{s}^{-1}$ )	$3.45 \times 10^{-5}$	$1.79 \times 10^{-5}$	$2.71 \times 10^{-5}$	$8.14 \times 10^{-7}$	$11.94 \times 10^{-7}$	$1.75 \times 10^{-7}$	$3.13 \times 10^{-6}$

below the Curie temperature of iron, we kept the chemical potential of iron in its ferromagnetic bcc state. We found an average formation energy of 0.75 eV for a C interstitial in an octahedral site and an average formation energy of 2.46 eV for a C interstitial in a T3 site in the paramagnetic (magnetic SQS) cementite. These formation energies are slightly above the ferromagnetic cases (0.64 and 2.39 eV, respectively), but the energy difference between the two interstitial sites is negligible. This energy difference is involved in various migration barriers. These results suggest that the present results on the C diffusion properties in the ferromagnetic cementite provide a rather satisfactory description of these properties in the paramagnetic cementite.

### C. Effect of alloying element on C interstitial diffusion

#### 1. Interaction between an alloying element (Mo,Cr,Mn) and a C interstitial

Mo, Mn, and Cr transition-metal solutes are known to favor the formation of carbides (for example, the cementite, the  $M_{23}C_6$ , etc.) in ferritic steels. The presence of an alloying element in  $\text{Fe}_3\text{C}$  can locally affect the energetic stability of the C octahedral interstitials and the migration energy barriers in the vicinity of the solute. In this second part of the paper, we investigate the impact of a substitutional Mo, Mn, or Cr in the metallic sub-lattice of cementite. As a first step, we focus on the rather dilute case. In practice, we replace one Fe atom by one solute in our supercell containing 96 metallic-atom sites.

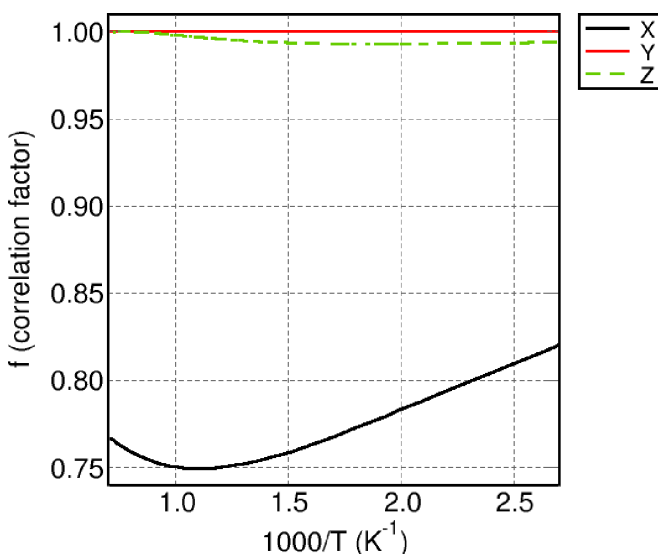


FIG. 5. Correlation factors for C diffusion on interstitial octahedral sites calculated in the x, y, and z directions.

The binding energy of a carbon interstitial-solute ( $\text{C}_{\text{int}}\text{-M}$ ) pair in  $\text{Fe}_{3n-1}\text{M}_1\text{C}_n$  cementite is given by:

$$E^b(\text{Fe}_{3n-1}\text{M}_1\text{C}_{n+1}) = E(\text{Fe}_{3n-1}\text{M}_1\text{C}_n) + E(\text{Fe}_{3n}\text{C}_{n+1}) - E(\text{Fe}_{3n-1}\text{M}_1\text{C}_{n+1}) - E(\text{Fe}_{3n}\text{C}_n) \quad (12)$$

with  $E(\text{Fe}_{3n-1}\text{M}_1\text{C}_n)$  and  $E(\text{Fe}_{3n}\text{C}_{n+1})$  the total energies of cementite, with a substitutional M or with a C interstitial, respectively.  $E(\text{Fe}_{3n}\text{C}_n)$  is the total energy of low-alloyed cementite with a C interstitial and  $E(\text{Fe}_{3n}\text{C}_n)$  is the total energy of  $\text{Fe}_3\text{C}$  cementite. This formula can be seen as the total energy of each individual reactant, minus the total energy of each product of a reaction. According to this definition, positive binding energy means attraction. We examined all possible octahedral C sites around the solute up to a 4.20 Å distance, and calculated the corresponding binding energies. The results are presented Fig. 6.  $\text{Mo}_I$  and  $\text{Mo}_{II}$  solute configurations provide both repulsive and attractive C interstitial sites. Mn solutes configurations produce some attractive sites for short solute -  $\text{C}_{\text{int}}$  distances. All Cr -  $\text{C}_{\text{int}}$  configurations have zero or negative binding energies, with the exception of a  $\text{Cr}_{II}$  -  $\text{C}_{\text{int}}$  close (1.90 Å) pair. Overall, all the absolute values of the calculated binding energies are rather small (lower than 0.14 eV).

In order to rationalize the binding behavior, we first investigated the role of the solute atomic size on its interaction with the C interstitial. To this end, we compared the changes in the Voronoi volumes of the substitutional sites in cementite. The volume variation of a given site, due to the presence of a  $\text{C}_{\text{int}}$  and a substitutional solute ( $\Delta V$ ), is given by

$$\Delta V = \Delta V_C + \Delta V_M, \quad (13)$$

with  $\Delta V_C$  the change of volume induced by the insertion of the C interstitial in  $\text{Fe}_3\text{C}$  and  $\Delta V_M$  the change of volume induced by the substitution of a Fe atom by solute M in a cementite cell containing a C interstitial. The results are shown in Fig. 7. The interaction of the Mo -  $\text{C}_{\text{int}}$  pairs is mostly governed by the size effect of the Mo solute, which has a significantly larger atomic radius than Fe. In Fig. 7, we clearly observe that the binding energy of the Mo -  $\text{C}_{\text{int}}$  pair increases with  $\Delta V_C$ . The substitution of Mo is favored in the dilatation sites caused by the  $\text{C}_{\text{int}}$  insertion. Overall, the Mo -  $\text{C}_{\text{int}}$  binding energy increases with  $\Delta V_C$  and  $\Delta V$ . It is worth comparing these results with the effects of Mo in bcc Fe. Liu *et al.* [61] used DFT to systematically investigate the effect of dilute substitutional solutes on an interstitial carbon in  $\alpha$ -Fe. They found that the interaction between Mo and a C octahedral interstitial up to the 4nn distance are repulsive, especially in the 1nn case. These results are also in agreement with Ref. [62]. In our study, we also found that at short distances  $\text{C}_{\text{int}}\text{-Mo}$  pairs in cementite are mostly repulsive, as

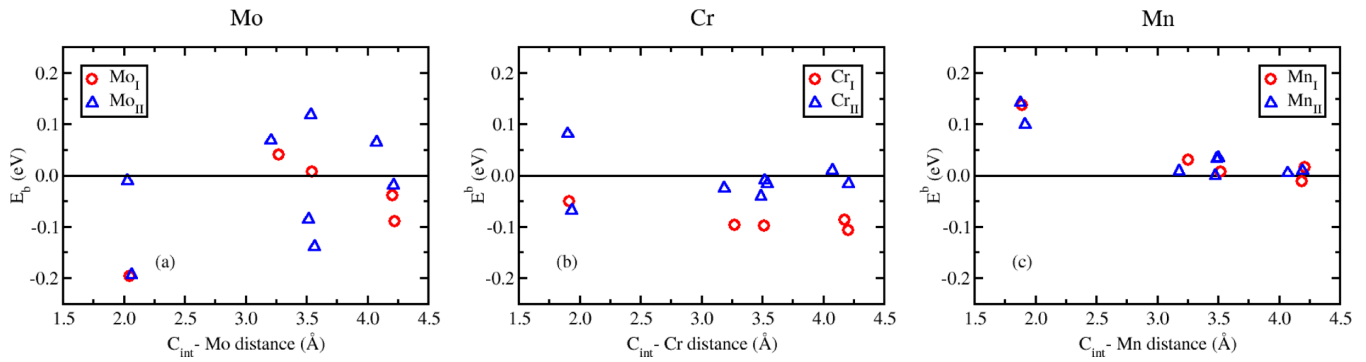


FIG. 6. Binding energies of the carbon interstitial-metallic solute pairs, up to a  $4.20\text{\AA}$   $C_{\text{int}}-M$  distance for  $M = \text{Mo}$  (a),  $\text{Cr}$  (b) and  $\text{Mn}$  (c). The two metallic sub-lattices of cementite ( $M_{\text{I}}$  and  $M_{\text{II}}$ ) are considered. According to the binding energy ( $E^b$ ) defined above, positive binding energies are associated with attractive pairs.

in bcc Fe, and we obtained some attractive C-Mo pairs for larger distances (between 3 and 4  $\text{\AA}$ ). At variance, in the case of a Mn solute, the binding energy of the solute - interstitial pair decreases with increasing  $\Delta V_C$ . Finally, we did not observe a Voronoi volume dependence for a Cr solute. Please note that, as Mn and Cr atoms admit a size close to that of iron atoms and the change of volume induced by the substitution is not significant ( $\Delta V \approx \Delta V_C$ ), and, the interaction between C and a Mn or Cr solute should be mostly governed by more complicated effects, such as magnetism or electronic charge redistribution.

The magnetic moment of a Mn solute in  $\text{Fe}_{95}\text{Mn}_1\text{C}_{32}$  is parallel to the Fe moments ( $1.90 \mu_B$  and  $1.57 \mu_B$  for  $\text{Mn}_{\text{I}}$  and  $\text{Mn}_{\text{II}}$  atoms, respectively). Cr solutes in the  $\text{Fe}_{95}\text{Cr}_1\text{C}_{32}$  system has a  $-0.82 \mu_B$  ( $\text{Cr}_{\text{I}}$ ) and  $-0.98 \mu_B$  ( $\text{Cr}_{\text{II}}$ ) antiferromagnetic with respect to the Fe spins. We investigated the change in Mn and Cr magnetic moments induced by the introduction of a C octahedral interstitial. In the case of a Mn solute, we observed a correlation between Mn- $C_{\text{int}}$  binding energy and the solute magnetic moment, as shown in Fig. 8: small  $\text{Mn}_{\text{I}}$  and  $\text{Mn}_{\text{II}}$  magnetic moments (which are closer to their respective moments far from the C interstitial) are associated with more significant binding energies, while higher Mn magnetic moments are associated with nearly zero binding energy pairs. This trend is fully consistent with the binding energy dependency on the  $\Delta V_C$ , because of the magnetovolume effect (see Fig. 8).

To further illustrate the relevant role of magnetism on the Mn- $C_{\text{int}}$  binding, we performed additional DFT calculations for the short Mn- $C_{\text{int}}$  distances ( $< 2 \text{\AA}$ ). We imposed the Mn solute magnetic moment to zero and relaxed the magnetic moments of all other atoms in cementite with or without a C interstitial. We replaced the total energies of the second and fourth terms of Eq. 12 by the total energies of the same cell with the zero-magnetic moment Mn. Overall, Mn magnetism enhances the Mn- $C_{\text{int}}$  attraction: if we constrain the moment of Mn to zero, the binding energy decreases by 0.12 eV for a  $\text{Mn}_{\text{I}}$  solute and by 0.07 eV for a  $\text{Mn}_{\text{II}}$  solute. The  $\text{Mn}_{\text{I}}$  are more penalized by turning-off its magnetism because its fully relaxed magnetic moment is larger, due to a smaller number of intrinsic C nearest neighbors, and consistently, a larger Voronoi volume.

In bulk Fe, according to theoretical studies [61–64], a Mn solute has a weak attractive interaction with its nearest C interstitial neighbor. This Mn- $C_{\text{int}}$  attractive interaction was also predicted by experimental studies [65,66]. In addition, nearest Mn- $C_{\text{int}}$  neighbors are associated with the largest compression site (lowest  $\Delta V_C$ ) and the lowest Mn ferromagnetic moment. This lowest magnetic moment is close to the metastable moment of an isolated ferromagnetic Mn in bulk bcc Fe [63]. We find indeed some similar behavior in the Mn-alloyed cementite: high binding energies correspond to short Mn- $C_{\text{int}}$  distances which themselves correspond to low Mn ferromagnetic moments.

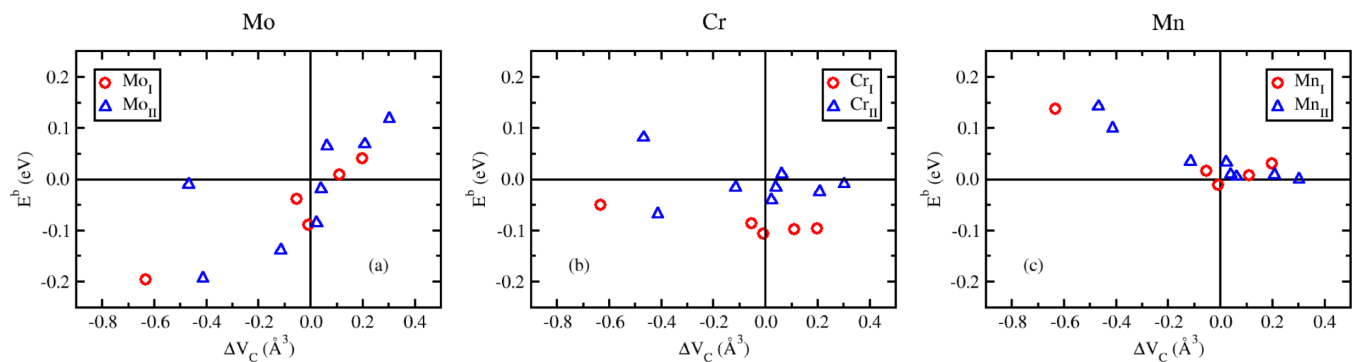


FIG. 7. [(a), (b) and (c)] Binding energies of an  $M$  ( $M=\text{Mo}$ ,  $\text{Cr}$ , and  $\text{Mn}$ , respectively) metallic solute - C octahedral interstitial pair in  $\text{Fe}_{95}M_1\text{C}_{33}$  vs the change in the substitutional site Voronoi volume induced by the insertion of the interstitial before the substitution ( $\Delta V_C$ ). The two metallic sublattices of cementite ( $M_{\text{I}}$  or  $M_{\text{II}}$ ) were considered. According to the binding energy ( $E^b$ ) defined above, positive binding energies are associated with attractive pairs.

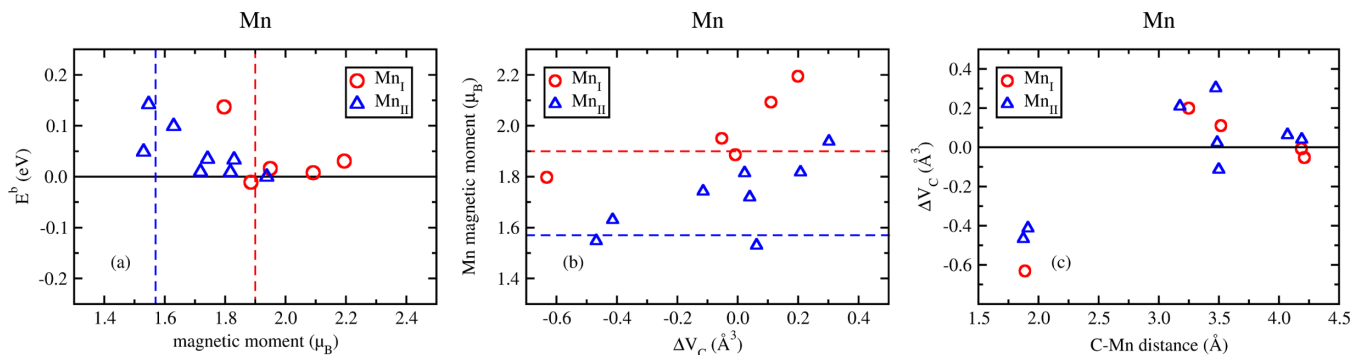


FIG. 8. (a) Binding energy of a C interstitial-Mn pair in  $\text{Fe}_{95}\text{Mn}_1\text{C}_{33}$  according to the magnetic moment of the Mn solute. (b) Magnetic moment of the Mn solute atom according to the change in the substitutional site Voronoi volume induced by the insertion of the C interstitial before the substitution ( $\Delta V_C$ ). (c) Change in the substitutional site Voronoi volume induced by the insertion of the C interstitial before substitution ( $\Delta V_C$ ) as a function of the C interstitial - Mn solute distance. The two metallic sub-lattices of cementite ( $M_I$  or  $M_{II}$ ) were considered. According to the binding energy ( $E^b$ ) defined above, positive binding energies are associated with attractive pairs. The red and blue dashed lines represent the magnetic moment of the  $Mn_I$  and a  $Mn_{II}$  (energetically most favorable) solute in bulk cementite, respectively.

Finally, in the case of a Cr solute,  $C_{\text{int}}$  - Cr pairs in cementite are all slightly repulsive or zero, with the exception of the shortest distance (Fig. 6). We did not evidence any clear trend of binding energy versus Cr magnetic moment. Cr solutes in the vicinity of a  $C_{\text{int}}$  ( $\text{Cr} - C_{\text{int}} < 2 \text{\AA}$ ) have very low magnetic moments (between  $-0.22\mu_B$  and  $0.12\mu_B$ ), while for larger distances, the Cr magnetic moment is close to the one in bulk  $\text{Fe}_{95}\text{Cr}_1\text{C}_{32}$ . In order to understand the attraction on the shortest Cr -  $C_{\text{int}}$  distance pair, we compared the partial density of state and differential charge density of various C-Cr distances. The study of the partial density of states of short ( $< 2 \text{\AA}$ ) Cr -  $C_{\text{int}}$  pairs established an hybridization between the solute  $3d$  states and the C  $2p$  states, as occurs for any close Fe-C pairs. However, in the only positive binding energy case (shortest Cr -  $C_{\text{int}}$  distance) we also observed an additional  $4s$ - $2p$  hybridization between the Cr solute and the C interstitial. This difference in the solute - interstitial hybridization is also reflected in the differential electronic charge density  $\Delta\rho$  induced by the C interstitial:

$$\Delta\rho = \rho(\text{Fe}_{95}\text{M}_1\text{C}_{32} + C_{\text{int}}) - \rho(\text{Fe}_{95}\text{M}_1\text{C}_{32}) - \rho(C), \quad (14)$$

with  $\rho(\text{Fe}_{95}\text{M}_1\text{C}_{32} + C_{\text{int}})$  the total charge density of cementite with a C interstitial and a substitutional atom M,  $\rho(\text{Fe}_{95}\text{M}_1\text{C}_{32})$  the total charge density of cementite with a substitutional M, and  $\rho(C)$  the total charge density of the C interstitial isolated. In Fig 9, we clearly see that in the configuration with the shortest Cr - C interstitial distance, the insertion of the interstitial induces an enhanced accumulation of charges in the Cr solute - C interstitial - Fe axis, in comparison with a repulsive Cr- $C_{\text{int}}$  pair configuration. Regarding the C interstitial - Cr solute pairs in bulk bcc Fe, first-principles studies [61,67] all predicted repulsive Cr -  $C_{\text{int}}$  interactions.

To summarize, the Mo -  $C_{\text{int}}$  and Mn- $C_{\text{int}}$  binding energies are dictated by the size effect and the solute magnetism, respectively, while the Cr -  $C_{\text{int}}$  attraction is rather due to a more subtle electronic hybridization effect.

## 2. C migration barrier in the vicinity of an alloying element

Although the binding energies found are not very large, the attractive sites may still act as traps for the diffusing C

interstitials. The presence of the solutes could locally induce a change of the C migration barriers. The most relevant C migration barriers to investigate are (i) barriers between two neighboring C attractive sites. If the barrier is rather low, the C interstitial can be caught in a cage movement. Such cage movements occur for instance during the migration of a C interstitial in  $\alpha$ -Fe in the vicinity of a vacancy [50]. (ii) The dissociation barriers for C to leave an attractive site. To determine if cage movements can appear in cementite with a Mo, Mn or Cr solute, we calculated the energy barriers between two neighboring attractive C octahedral sites in the vicinity of a substitutional solute. For each set of initial and final positions with non-negligible binding energies ( $E^b \geq 0.05 \text{ eV}$ ), we considered the lowest energy migration path in pure  $\text{Fe}_3\text{C}$  cementite, and calculated the new energy barrier, impacted by the nearby substitutional solute. Results are shown in Table VI. Overall, the migration barriers associated with neighboring attractive sites in the alloyed cementite are never significantly lower than the corresponding migration barriers in pure Fe cementite. No significant cage movement was identified. Since we found only one attractive site in the Cr-alloyed cementite case, we did not investigate cage movement in the vicinity of a Cr solute.

We also investigated the energetic barriers in the case of a dissociative migration. Due to the significant number of attractive sites induced by the presence of a Mo, Mn, or Cr solute in cementite, as well as the numerous possible jumps from each attractive site to a nonattractive site, we could not compute all the migration barriers associated with a dissociation. We therefore chose to focus on dissociative migrations between the most attractive sites and a zero (or almost zero) binding energy sites. We prioritized the calculations of energy barriers linked with a direct migration path along the x and z axis (the Octa - T3 - T2 - Octa movement described previously), because those are the lowest in  $\text{Fe}_3\text{C}$ . A nonexhaustive list of some possible energy barriers associated with dissociation movements is given in Table VII. Similarly to energy barriers associated with potential cage movement, the energy barriers associated with dissociative jumps in the case of Mo or Cr are approximately the same as in pure Fe cementite. However, in the case of a Mn solute, some energy barriers are

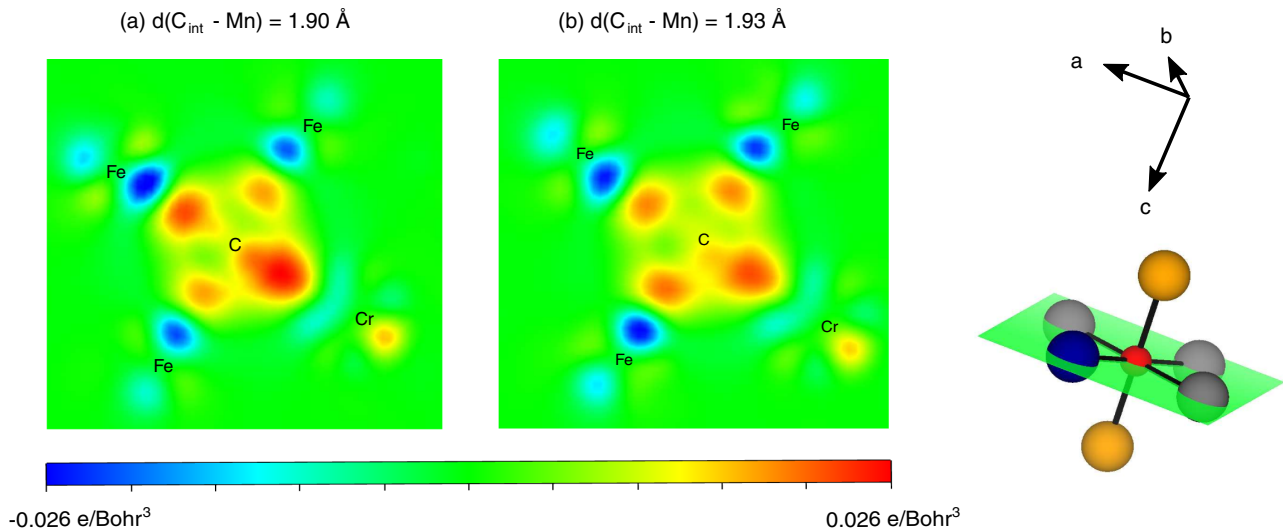


FIG. 9. Charge density differences induced by the insertion of a C interstitial in  $\text{Fe}_{95}\text{Cr}_1\text{C}_{32}$ , for two close Cr solute - C interstitial pairs. (a) is the lowest C interstitial - Cr solute distance possible in cementite, with an attractive binding energy. (b) is a repulsive configuration. The corresponding plane of the octahedral cite is represented on the left. As in Fig. 1,  $\text{Fe}_I$  atoms are in orange, while  $\text{Fe}_{II}$  atoms are in grey. The Cr solute is in blue, while the C interstitial octahedral site is in red.

slightly lower than in  $\text{Fe}_3\text{C}$ . Considering the calculated binding energies and barriers, we would not expect a significant effect of alloying elements on the C diffusion (at least in the dilute regime), except maybe in the presence of Mn, which is confirmed below.

### 3. Effects of the substitutional solutes on C diffusion in cementite

In the previous sections, we have presented the binding energy between an interstitial C atom and a substitutional solute (Mo, Cr, or Mn), as well as the carbon migration energies around the solutes. In this section, we use these data as inputs for the KINECLUE code [23] to quantify the effect of the solute addition on carbon diffusion in cementite. Assumptions and calculation details for the determination of C diffusivity around solutes are explained in Sec. II B.

For each of the three solutes Mn, Mo, and Cr, Fig. 10 shows the effect of their on the diffusivity of C atoms in cementite, as a function of temperature and the solute concentration. The quantity  $\delta D_C$  plotted on those graphs is the normalized difference between the carbon diffusion coefficients with and without the presence of the substitutional solute:

$$\delta D_C = \frac{\bar{D}_C([\bar{M}]) - D_C}{D_C}. \quad (15)$$

TABLE VI. Migration energy barriers between two neighboring attractive C octahedral interstitials in cementite with a Mo, Mn, or Cr solute. The binding energies before (initial) and after (final) the C jump are given at constant pressure (Pct) and at constant volume (Vct) at which the NEB calculations were performed.

Type of metallic solute	Binding energies (eV) initial/final Pct (Vct)	Jump mechanism (barrier in unalloyed $\text{Fe}_3\text{C}$ )	Energy barrier in alloyed $\text{Fe}_3\text{C}$ (forward/backward) (eV)
$\text{Mo}_I$	0.04/0.04 (−0.01/−0.01)	Indirect mechanism along y axis (2.16 eV)	2.25
$\text{Mo}_{II}$	0.12/0.07 (0.08/0.02)	Direct mechanism along the xz plane (2.13 eV)	2.14/2.08
$\text{Mn}_I$	0.10/0.10 (0.09/0.09)	Indirect mechanism along y axis (2.16 eV)	2.44
$\text{Mn}_{II}$	0.12/0.07 (0.08/0.05)	Direct mechanism along the xz plane (2.13 eV)	2.31/2.28

We considered solute concentrations up to a few at.%. Overall, the influence of the alloying elements on C diffusivity is small, in weakly alloyed cementites. Mn is the solute with the most visible effect: C diffusion can be slowed down by a factor of 10 approximately at low temperatures (<500 K) and in the presence of 1% of Mn and beyond. This can be expected because only the Mn solute has the most various attractive sites in its nearest-neighbor region, where the C interstitial can jump from one of these sites to another. This can induce some small trapping effects. In that respect, we found that dissociative jumps energy barriers are slightly higher in the case of Mn solute (see Table VII).

It is worth mentioning that, according to CALPHAD (CALculation of PHase Diagrams) data, cementite precipitates can indeed be present in Fe-Mn-C alloys. Using THERMO-CALC commercial software [68,69] with the TCFE Steels/Fe-alloy version-10 database, we investigated the phases of Fe-Mn-C systems with a nominal Mn concentration up to approximately 5 at.%. For temperatures at which we predicted a visible influence of Mn on C diffusivity, the predicted Mn concentration in cementite phases is between 4 at.% and 23 at.% at 450 K and between 2 at.% and 30 at.% at 500 K, for low (<2 %) Mn nominal concentrations. Our

TABLE VII. Migration energy barriers associated with a dissociative jump in cementite around a Mo, Mn, or Cr solute. The binding energies before (initial) and after (final) the C jump are given at constant pressure (Pct) and at constant volume (Vct) at which the NEB calculations were performed.

Type of metallic solute	Binding energies (eV) initial/final Pct (Vct)	Jump mechanism (barrier in unalloyed Fe <sub>3</sub> C)	Energy barrier in alloyed Fe <sub>3</sub> C (eV) (forward/backward)
Mo <sub>II</sub>	0.12/−0.01 (0.08/−0.08)	Direct mechanism along the <i>xz</i> plane (2.13 eV)	1.92/1.76
Mo <sub>II</sub>	0.12/0.00 (0.08/−0.05)	Indirect mechanism along <i>y</i> axis (2.16 eV)	2.28/2.16
Mo <sub>II</sub>	0.12/0.00 (0.08/−0.15)	Indirect mechanism along <i>y</i> axis (2.16 eV)	2.25/2.01
Mn <sub>I</sub>	0.14/0.01 (0.09/−0.04)	Direct mechanism along the <i>xz</i> plane (2.13 eV)	2.21/2.09
Mn <sub>II</sub>	0.14/0.00 (0.08/−0.05)	Direct mechanism along the <i>xz</i> plane (2.13 eV)	2.19/2.05
Mn <sub>II</sub>	0.14/−0.01 (0.08/−0.04)	Direct mechanism along the <i>xz</i> plane (2.13 eV)	2.12/1.99
Cr <sub>II</sub>	0.08/−0.01 (0.02/−0.05)	Direct mechanism along the <i>xz</i> plane (2.13 eV)	2.14/2.07
Cr <sub>II</sub>	0.08/0.01 (0.02/−0.04)	Direct mechanism along the <i>xz</i> plane (2.13 eV)	2.14/2.08

current results suggest a decrease of C diffusion coefficients in these Mn-alloyed cementite. However, please note that our method used for the determination of C diffusion coefficients (with the KINECLUE code) is only accurate for small alloying element concentrations (up to a few percents at most). For higher concentrations, interactions between Mn solutes would need to be considered, but this goes beyond the scope of the present study.

#### IV. CONCLUSION

We have investigated the diffusion of carbon in pure and weakly alloyed cementite, respectively Fe<sub>3</sub>C and (Fe<sub>1−*x*</sub>M<sub>*x*</sub>)<sub>3</sub>C with *M* = Mo, Cr, or Mn. Systematic DFT calculations were performed to determine the formation energy of all identified single C interstitials, as well as the energy

barrier of a large variety of jumps between the lowest-energy C interstitial configurations. Then, the KineCluE code was used to compute carbon diffusion coefficients in cementite using the DFT energetics as input data.

The obtained values in Fe<sub>3</sub>C are in satisfactory agreement with experiments measuring the growth rate of cementite, for example on top of a ferritic substrate. Indeed, in such experiments, carbon diffusion was assumed as the rate-limiting mechanism governing the growth of cementite. The present study provides information on carbon migration mechanisms at the atomic scale, which is not directly accessible by experiments. We highlighted two elementary diffusion mechanisms: either a direct jump of a C interstitial from one octahedral site to another one, or an indirect jump where the C interstitial moves and takes the place of an intrinsic C, and the latter migrates towards an interstitial site.

It is interesting to note that although our predicted diffusion coefficients are comparable to the values from the previous semiempirical MD simulation, the mechanisms at their origin are different. Indeed, the mechanism previously inferred from MD simulations relies on a high concentration of C Frenkel pairs. With a higher C Frenkel pair formation energy, the MD based mechanism has a lower probability to occur. Alternatively, the present study proposes C to diffuse via interstitial mechanisms, involving jumps between octahedral interstitial sites. Note that in those carburization experiments, the vapor phase acts as a source to provide C interstitials leading to the growth of cementite, the formation energy associated with the creation of interstitial C atoms is not involved in the activation energy of this process.

In order to investigate possible effects of the alloying elements (Mo, Cr, and Mn) on the diffusion properties of C, we first calculated and analyzed the interaction energy between a C interstitial and one of the three substitutional solutes. Some energetically favorable sites are found for a C interstitial around the solutes. The location of these sites are governed by the solute size effect, the solute magnetism and the electronic charge redistribution, for the Mo, Mn, and Cr case, respectively.

Regarding the influence of substitutional solutes on the C diffusion coefficients, we found that Mn decreases C diffusion coefficients by at most a factor of 10 at temperatures up to 500 K and solute concentrations up to a few at%.

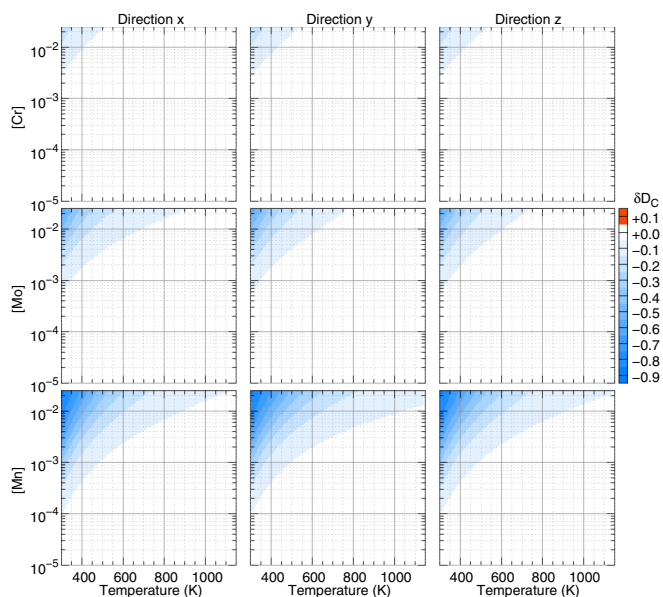


FIG. 10. Effect of substitutional solutes Mo, Mn, and Cr on the diffusion coefficient of carbon in cementite. The normalized difference between the carbon diffusion coefficients with and without the presence of the substitutional solute  $\delta D_C$  [defined in Eq. (15)] is plotted as a function of the temperature and the solute concentration.

Mo and Cr, we predict no visible effects within the considered weakly alloyed conditions.

Finally, this combined first-principles and the KineCluE modeling offers an accurate and efficient atomistic approach for the study of atomic transport in solid systems with a relatively low symmetry.

As a first step in the investigation of diffusion in cementite, this study considers stoichiometric cementite ( $M_3C$ ). However, according to both experimental and theoretical studies [70], C vacancy concentration in cementite could reach up to a few percent. The vacancies might play a significant role on

C diffusion, which is undeniably an interesting perspective for a future study.

#### ACKNOWLEDGMENTS

We thank A. Benarosch and C. Toffolon for fruitful discussions. First-principles calculations were performed using Grand Equipement National de Calcul Intensif (GENCI) resources under the No. A0070906020 and No. A0090906020 Projects and the CINECA-MARCONI supercomputer within the SISTEEL project.

- 
- [1] Z. Yang, S. Jin, L. Song, W. Zhang, L. You, and L. Guo, *Metals* **8**, 349 (2018).
- [2] S. Klein, L. M. Roncery, M. Walter, S. Weber, and W. Theisen, *J. Mater. Sci.* **52**, 375 (2016).
- [3] W. Kesternich and R. Nandedkar, *J. Nucl. Mater.* **179**, 1015 (1991).
- [4] S. Kano, H. Yang, J. Shen, Z. Zhao, J. McGrady, D. Hamaguchi, M. Ando, H. Tanigawa, and H. Abe, *J. Nucl. Mater.* **502**, 263 (2018).
- [5] M. Hillert and M. Sharp, *Jernkontorets Ann.* **137**, 785 (1953).
- [6] B. Ozturk, V. L. Fearing, J. A. Ruth, and G. Simkovich, *Metall. Trans. A* **13**, 1871 (1982).
- [7] J. R. B. Ozturk, V. Fearing, and G. Simkovich, *Solid State Ionics* **12**, 145 (1984).
- [8] A. Schneider and G. Inden, *Calphad* **31**, 141 (2007).
- [9] I. B. E. Levchenko, A. Evteev, and G. Murch, *Acta Mater.* **57**, 846 (2009).
- [10] C. Jiang, B. Uberuaga, and S. Srinivasan, *Acta Mater.* **56**, 3236 (2008).
- [11] M. Umemoto, Z. Liu, K. Masuyama, and K. Tsuchiya, *Scr. Mater.* **45**, 391 (2001).
- [12] P. E. Blöchl, *Phys. Rev. B* **50**, 17953 (1994).
- [13] G. Kresse and J. Hafner, *Phys. Rev. B* **47**, 558 (1993).
- [14] G. Kresse and J. Furthmüller, *Comput. Mater. Sci.* **6**, 15 (1996).
- [15] G. Kresse and J. Furthmüller, *Phys. Rev. B* **54**, 11169 (1996).
- [16] J. P. Perdew, K. Burke, and M. Ernzerhof, *Phys. Rev. Lett.* **77**, 3865 (1996).
- [17] H. J. Monkhorst and J. D. Pack, *Phys. Rev. B* **13**, 5188 (1976).
- [18] M. Methfessel and A. T. Paxton, *Phys. Rev. B* **40**, 3616 (1989).
- [19] H. Jónsson, G. Mills, and K. W. Jacobsen, *Nudged Elastic Band Method for Finding Minimum Energy Paths of Transitions* (World Scientific, 1989).
- [20] G. Henkelman, B. P. Uberuaga, and H. Jónsson, *J. Chem. Phys.* **113**, 9901 (2000).
- [21] G. H. Vineyard, *J. Phys. Chem. Solids* **3**, 121 (1957).
- [22] A. Togo and I. Tanaka, *Scr. Mater.* **108**, 1 (2015).
- [23] T. Schuler, L. Messina, and M. Nastar, Kineclue v1.0 github repository (2019).
- [24] T. Schuler, L. Messina, and M. Nastar, *Comput. Mater. Sci.* **172**, 109191 (2019).
- [25] M. Nastar, V. Y. Dobretsov, and G. Martin, *Philos. Mag. A* **80**, 155 (2000).
- [26] L. Messina, T. Schuler, M. Nastar, M.-C. Marinica, and P. Olsson, *Acta Mater.* **191**, 166 (2020).
- [27] T. Schuler, M. Nastar, and L. Messina, *Phys. Rev. Materials* **4**, 020401(R) (2020).
- [28] O. Barbour, J. P. Crocombette, T. Schuler, and M. Tupin, *J. Nucl. Mater.* **539**, 152333 (2020).
- [29] T. Schuler, C. Barouh, M. Nastar, and C.-C. Fu, *Phys. Rev. Lett.* **115**, 015501 (2015).
- [30] W. Chiou, *Surf. Sci.* **530**, 88 (2003).
- [31] D. Walker, J. Li, B. Kalkan, and S. M. Clark, *Am. Mineral.* **100**, 2610 (2015).
- [32] A. Tsuzuki, S. Sago, S. I. Hirano, and S. Naka, *J. Mater. Sci.* **19**, 2513 (1984).
- [33] H. jin Choe, T. Terai, T. Fukuda, T. Kakeshita, S. Yamamoto, and M. Yonemura, *J. Magn. Magn. Mater.* **417**, 1 (2016).
- [34] S. W. J. Smith, W. White, and S. G. Barker, *Proc. Phys. Soc. London* **24**, 62 (1911).
- [35] L. J. E. Hofer and E. M. Cohn, *J. Am. Chem. Soc.* **81**, 1576 (1959).
- [36] A. Schneider, C.-C. Fu, F. Soisson, and C. Barreateau, *Phys. Rev. Lett.* **124**, 215901 (2020).
- [37] V. Razumovskiy and G. Ghosh, *Comput. Mater. Sci.* **110**, 169 (2015).
- [38] Z. Lv, F. Zhang, S. Sun, Z. Wang, P. Jiang, W. Zhang, and W. Fu, *Comput. Mater. Sci.* **44**, 690 (2008).
- [39] H. I. Faraoun, Y. D. Zhang, C. Esling, and H. Aourag, *J. Appl. Phys.* **99**, 093508 (2006).
- [40] C. Jiang, S. G. Srinivasan, A. Caro, and S. A. Maloy, *J. Appl. Phys.* **103**, 043502 (2008).
- [41] M. Nikolussi, S. Shang, T. Gressmann, A. Leineweber, E. Mittemeijer, Y. Wang, and Z.-K. Liu, *Scr. Mater.* **59**, 814 (2008).
- [42] A. Dick, F. Körmann, T. Hickel, and J. Neugebauer, *Phys. Rev. B* **84**, 125101 (2011).
- [43] K. O. E. Henriksson, N. Sandberg, and J. Wallenius, *Appl. Phys. Lett.* **93**, 191912 (2008).
- [44] J. Häglund, G. Grimvall, and T. Jarlborg, *Phys. Rev. B* **44**, 2914 (1991).
- [45] F. H. Herbstein and J. Smuts, *Acta Crystallogr.* **17**, 1331 (1964).
- [46] J. Li, H. K. Mao, Y. Fei, E. Gregoryanz, M. Erements, and C. S. Zha, *Phys. Chem. Miner.* **29**, 166 (2002).
- [47] E. J. Fasiska and G. A. Jeffrey, *Acta Crystallogr.* **19**, 463 (1965).
- [48] I. G. Wood, L. Vočadlo, K. S. Knight, D. P. Dobson, W. G. Marshall, G. D. Price, and J. Brodholt, *J. Appl. Crystallogr.* **37**, 82 (2004).
- [49] S. Ahlawat, K. Srinivasu, A. Biswas, and N. Choudhury, *Comput. Mater. Sci.* **170**, 109167 (2019).

- [50] C. Barouh, T. Schuler, C.-C. Fu, and T. Jourdan, *Phys. Rev. B* **92**, 104102 (2015).
- [51] D. E. Jiang and E. A. Carter, *Phys. Rev. B* **67**, 214103 (2003).
- [52] C. Domain, C. S. Becquart, and J. Foct, *Phys. Rev. B* **69**, 144112 (2004).
- [53] D. Simonovic, C. K. Ande, A. I. Duff, F. Syahputra, and M. H. F. Sluiter, *Phys. Rev. B* **81**, 054116 (2010).
- [54] J. da Silva and R. B. McLellan, *Mater. Sci. Eng.* **26**, 83 (1976).
- [55] W. Pascheto and G. P. Johari, *Metall. Mater. Trans. A* **27**, 2461 (1996).
- [56] Y. Iijima, *J. Alloys Compd.* **234**, 290 (1996).
- [57] *Diffusion in Solid Metals and Alloys*, edited by H. Mehrer (Springer-Verlag, Berlin, 1990).
- [58] A. Lord and D. Beshers, *Acta Metall.* **14**, 1659 (1966).
- [59] C. A. Wert, *Phys. Rev.* **79**, 601 (1950).
- [60] R. McLellan and M. Wasz, *J. Phys. Chem. Solids* **54**, 583 (1993).
- [61] P. Liu, W. Xing, X. Cheng, D. Li, Y. Li, and X.-Q. Chen, *Phys. Rev. B* **90**, 024103 (2014).
- [62] A. Bakaev, D. Terentyev, G. Bonny, T. Klaver, P. Olsson, and D. V. Neck, *J. Nucl. Mater.* **444**, 237 (2014).
- [63] A. Schneider, C.-C. Fu, and C. Barreteau, *Phys. Rev. B* **98**, 094426 (2018).
- [64] N. I. Medvedeva, D. C. V. Aken, and J. E. Medvedeva, *J. Phys.: Condens. Matter* **23**, 326003 (2011).
- [65] H. Abe, T. Suzuki, and S. Okada, *Trans. Jpn. Inst. Met.* **25**, 215 (1984).
- [66] V. Massardier, J. Merlin, E. L. Patezour, and M. Soler, *Metall. Mater. Trans. A* **36**, 1745 (2005).
- [67] N. Sandberg, K. O. E. Henriksson, and J. Wallenius, *Phys. Rev. B* **78**, 094110 (2008).
- [68] J.-O. Andersson, T. Helander, L. Höglund, P. Shi, and B. Sundman, *Calphad* **26**, 273 (2002).
- [69] ThermoCalc, website 2020, <https://thermocalc.com/>, accessed: 2010-12-20.
- [70] A. Leineweber, S. Shang, and Z. Liu, *Acta Mater.* **86**, 374 (2015).